

Field-induced states and thermodynamics of the frustrated Heisenberg antiferromagnet on a square lattice

Andreas Honecker,¹ M. E. Zhitomirsky,² Alexander Wietek,³ and Johannes Richter^{3,4}

¹*Laboratoire de Physique Théorique et Modélisation,*

CNRS UMR 8089, CY Cergy Paris Université, Cergy-Pontoise, France

²*Université Grenoble Alpes, CEA, IRIG, PHELIQS, 38000 Grenoble, France*

³*Max-Planck-Institut für Physik Komplexer Systeme, Nöthnitzer Straße 38, 01187 Dresden, Germany*

⁴*Institut für Theoretische Physik, Otto-von-Guericke-Universität Magdeburg, 39016 Magdeburg, Germany*

(Dated: January 12, 2026)

We investigate the ground-state and finite-temperature properties of the J_1 - J_2 Heisenberg antiferromagnet on the square lattice in the presence of an external magnetic field. We focus on the highly frustrated regime around $J_2 \approx J_1/2$. The h - T phase diagram is investigated with particular emphasis on the finite-temperature transition into the “up-up-up-down” state that is stabilized by thermal and quantum fluctuations and manifests itself as a plateau at one half of the saturation magnetization in the quantum case. We also discuss the enhanced magnetocaloric effect associated to the ground-state degeneracy that arises at the saturation field for $J_2 = J_1/2$. For reference, we first study the classical case by classical Monte Carlo simulations. Then we turn to the extreme quantum limit of spin-1/2 where we perform zero- and finite-temperature Lanczos calculations.

I. INTRODUCTION

The Heisenberg antiferromagnet with nearest-neighbor, $J_1 > 0$, and next-nearest-neighbor bonds, $J_2 \geq 0$, called J_1 - J_2 model, or frustrated square lattice antiferromagnet (FSAFM), is the archetypical frustrated spin model [1, 2]. The corresponding Hamiltonian is given by

$$\mathcal{H} = J_1 \sum_{\langle i,j \rangle} \mathbf{s}_i \cdot \mathbf{s}_j + J_2 \sum_{\langle\langle i,j \rangle\rangle} \mathbf{s}_i \cdot \mathbf{s}_j - h \sum_i s_i^z \quad (1)$$

including a coupling with an applied magnetic field h . Here, $\langle \cdot, \cdot \rangle$ denotes summation over the nearest-neighbor bonds J_1 whereas $\langle\langle \cdot, \cdot \rangle\rangle$ corresponds to the next-nearest neighbor J_2 bonds that couple spins on the diagonals of square plaquettes.

The J_1 - J_2 square-lattice model was introduced in the late 1980s with the aim to describe the breakdown upon doping of Néel antiferromagnetic (NAF) state in the high-temperature cuprate superconductors [3–5]. Over the last few decades the zero-field case, $h = 0$, has attracted much attention, since it is a canonical model to study frustration-induced quantum phase transitions between semiclassical ground-state phases with a magnetic long-range order (LRO) and disordered quantum phases, see, e.g., Refs. [3–59].

Based on numerous studies using a plethora of quantum many-body methods, consensus has been achieved that the J_1 - J_2 model in the extreme quantum limit $s = 1/2$ exhibits a magnetically disordered spin-rotation-invariant quantum phase in a small region $J_2^{c1} < J_2 < J_2^{c2}$ around $J_2 = 0.5J_1$. The semi-classical ground-state phases of the model, namely the Néel antiferromagnetic LRO at small $J_2/J_1 < J_2^{c1}$ and the collinear antiferromagnetic LRO at large $J_2/J_1 > J_2^{c2}$, are well understood. Concerning the critical values J_2^{c1} and J_2^{c2} , some estimates are $J_2^{c1} = 0.44 - 0.46$ and $J_2^{c2} = 0.59 - 0.5$ [20, 32, 36, 37, 40, 44, 47, 59]. However, some recent

PEPS approaches [38, 41, 42, 52] lead to a transition point J_2^{c1} close to 0.5 or even above. Concerning the nature of the intermediate magnetically disordered quantum phase, there is an ongoing active controversial debate [17, 20, 26–42, 44–46, 48, 50, 52, 58]. A particular controversy concerns the very existence of an excitation gap in the intermediate quantum phase. A finite excitation gap was reported in Refs. [23, 27, 28, 33], whereas indications of a gapless spin liquid state were found in Refs. [29, 30, 36, 50]. Investigations based on density matrix renormalization group with explicit implementation of $SU(2)$ spin rotation symmetry in Ref. [32] report on a gapless spin liquid for $0.44 < J_2/J_1 < 0.5$ and a gapped plaquette valence bond phase for $0.5 < J_2/J_1 < 0.61$. This structure of the phase diagram is reaffirmed in Ref. [50], but the point separating the two intermediate phases is shifted to $J_2/J_1 \approx 0.56$. On the other hand, a recent matrix-product state method claims that there is no spin-liquid phase in this model [52].

In addition to the basic theoretical interest in this nontrivial quantum many-body model, it also attracts attention thanks to its relation to experimental studies of various magnetic materials, such as VOMoO_4 [60], $\text{Li}_2\text{VOSiO}_4$ and $\text{Li}_2\text{VOGeO}_4$ [61–63], $\text{BaCdVO}(\text{PO}_4)_2$ [64], $\text{RbMoOPO}_4\text{Cl}$ [65], SrLaCuSbO_6 and SrLaCuNbO_6 [66], $\text{NaZnVOPO}_4(\text{HPO}_4)$ [67], YbBi_2IO_4 and $\text{YbBi}_2\text{ClO}_4$ [68], and KMPO_4 [69, 70]. However, to the best of our knowledge so far no magnetic material with an exchange-parameter ratio J_2/J_1 suitable for a magnetically disordered ground-state phase has been found.

The unconventional quantum nature of the zero-field ground state in the strong-frustration regime has also stimulated the search for unconventional features in the magnetization curve [71–82] as well as finite-temperature properties [83–91] of the spin-1/2 FSAFM. In particular, in the regime of strong frustration $J_2/J_1 \approx 0.5$, where the zero-field quantum ground state does not exhibit mag-

netic LRO, evidence for a well-pronounced plateau at 1/2 of saturation was found [72].

In this paper, we revisit the behavior of the frustrated square-lattice antiferromagnet in an external magnetic field at zero and at finite temperature, where we focus on the regime around $J_2/J_1 = 0.5$. In Sec. II we first revisit the h - T phase diagram of the classical Heisenberg model at $J_2/J_1 = 0.5$. Then, in Sec. III we switch to the extreme quantum limit of spin $s = 1/2$. We first revisit the zero-temperature phase diagram in an external field in Subsec. III A and then study finite-temperature properties in an external field in Subsec. III B. Finally, we conclude in Sec. IV with a Summary and perspectives. We note that while much of the work on the spin-1/2 model focusses on the controversial $h = 0, T = 0$ phase diagram in the regime around $J_2/J_1 = 0.5$, here we do *not* intend to contribute to this particular question that is intensively studied by many other authors, as reviewed above.

II. CLASSICAL MODEL

A. Ground states

We begin with the classical J_1 - J_2 model (1) treating spins \mathbf{s}_i as three-component unit vectors. For a special ratio of the two exchange constants $J_2/J_1 = 1/2$, magnetic frustration is enhanced featuring an infinite classical degeneracy for all magnetic fields below the saturation [72]. In order to see this we define a total spin of a square plaquette α :

$$\mathbf{L}_\alpha = \sum_{i \in \alpha} \mathbf{s}_i, \quad (2)$$

as a sum over four surrounding sites. Then, for $J_2 = J_1/2$, the spin Hamiltonian (1) can be rewritten as a function of \mathbf{L}_α variables only

$$\mathcal{H} = \frac{1}{4} \sum_\alpha \left(J_1 \mathbf{L}_\alpha^2 - h L_\alpha^z \right). \quad (3)$$

So far, this is an exact transformation valid for any value of the spin. Let us now focus on the classical case. Minimizing energy of a single square plaquette we obtain from Eq. (3):

$$L_\alpha^z = h/(2J_1). \quad (4)$$

Any classical spin configuration that satisfies the above constraint for *every* square plaquette yields the lowest ground-state energy. The subsequent analysis of degenerate ground states splits into two parts: (i) finding equilibrium four-sublattice configurations for one block and (ii) extending single-block states to the entire lattice. Before doing that we note that the constraint (4) gives the following equilibrium magnetization $m = L_\alpha^z/4 = h/(8J_1)$, which in turn yields for the saturation field $h_{\text{sat}} = 8J_1$.

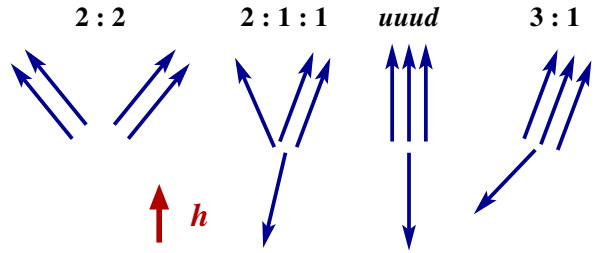


FIG. 1. Spin configurations minimizing the classical energy of a single four-site plaquette of the FSAFM in different magnetic fields. The collinear *uuud* state produces the 1/2 magnetization plateau.

At $T = 0$, the classical magnetization curve $m(h)$ is a straight line up to h_{sat} .

The constraint (4) imposes three conditions on the eight angle variables for the four spins of each block. One more angle variable is eliminated by the broken $O(2)$ rotation symmetry about the field direction. Overall, this counting yields four continuous variables to describe various classical ground states for a single block. Analysis of the effect of fluctuations, thermal or quantum, on a state selection can be performed using the concept of an effective biquadratic exchange, see, for example, Ref. [92]. Figure 1 sketches the relevant spin configurations that appear for four site blocks in various magnetic fields [72, 93, 94]. The “up-up-up-down” (*uuud*) configuration has the lowest energy for magnetic fields around $h_{\text{sat}}/2$ and produces the magnetization plateau with $m = 1/2$. At higher fields away from the 1/2 plateau, spins tilt retaining the 3:1 splitting. For fields below $m < 1/2$, the noncollinear spin configuration has a more complex 2:1:1 structure. The 2:2 state, which is one of the classical ground states in the entire range $0 < h < h_{\text{sat}}$, is stable, in the presence of a biquadratic exchange, in the low-field region only [94].

Since the plaquettes α share edges, one spin participates in several plaquettes. As a result, one faces the problem of extending a single block solution to the entire lattice. This leads to additional degeneracy for the lattice spin model for each of the single block solutions in Fig. 1. The corresponding degeneracy is most easily visualized for the *uuud* state [72]. Specifically, consider the most symmetric *uuud* configuration. For that we choose the down spin, for example, in the lowest left corner of the first square plaquette and extend this configuration in a translationally invariant way over the whole lattice. This state consists of parallel, vertical and horizontal, lines of up-down spins separated by lines of up spins. The alternating up-down spins along any of these lines can be freely rotated around an arbitrary angle without changing the total classical energy [72]. Since the *uuud* state permits a maximum of such deformations, one may expect it to be selected by thermal fluctuations via the “order-by-disorder” mechanism [95–100]. A subtle prop-

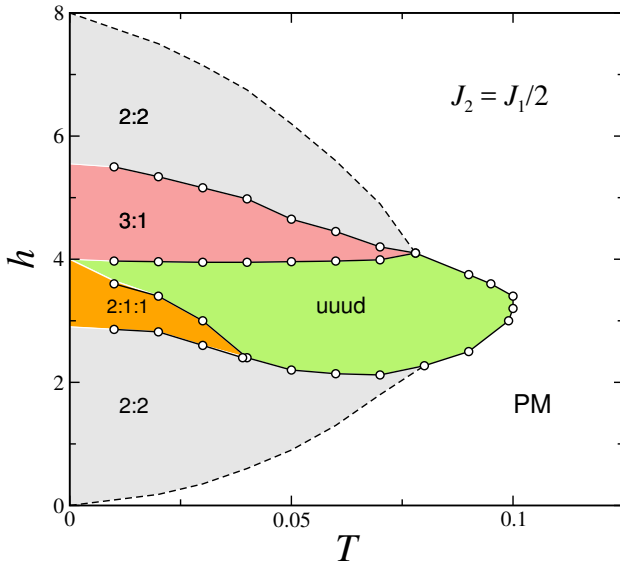


FIG. 2. Field-temperature phase diagram of the classical FSAFM with $J_2 = 0.5$, $J_1 = 1$. Magnetic states with (quasi) LRO are labeled according to Fig. 1, PM stands for a disordered paramagnetic state. Phase transition points obtained from the Monte Carlo simulations are shown by open circles with solid lines as a guide for the eye. The dashed lines indicate the expected Berezinskii-Kosterlitz-Thouless transition boundaries.

erty of the order-by-disorder mechanism is a competition between a local fluctuation contribution manifested by the effective biquadratic coupling and the extended zero-energy modes related to spin distribution over the entire lattice. Furthermore, in the latter case there is the possibility of distinct effects from the thermal fluctuations, which rely on the entropic contribution of the low-energy (zero) modes, and from the quantum fluctuations, with magnons at different momenta contributing equally. As we shall see below, all these exotic features of the order-by-disorder effect are relevant for the FSAFM.

B. Field-temperature phase diagram

Next, we present new classical Monte-Carlo results on significantly larger lattices compared to the previous studies [72, 74]. Simulations have been performed using the single-spin flip Metropolis algorithm in combination with the microcanonical over-relaxation moves. Details of the algorithm are provided in recent studies devoted to various classical frustrated spin models [101–103].

Figure 2 presents the constructed h - T phase diagram for $J_2/J_1 = 1/2$. First, we observe the expected stabilization of the *uuud* phase by thermal fluctuations in the regime $T \lesssim J_1/10$. The stability region is asymmetric around $h_c = 0.5h_{\text{sat}}$ having a significant extent into the low-field part of the diagram. Second, there are sizable regions with the 2:1:1 and 3:1 states just below or above

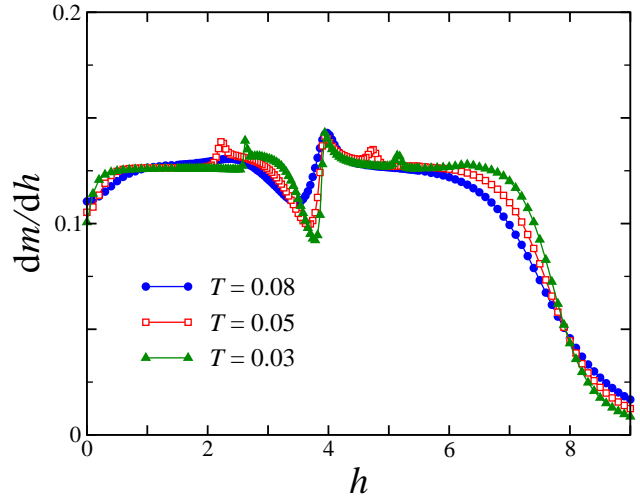


FIG. 3. The field derivative of the magnetization for the classical FSAFM with $J_2 = 0.5$, $J_1 = 1$ at three different temperatures obtained on lattices with $L = 32$.

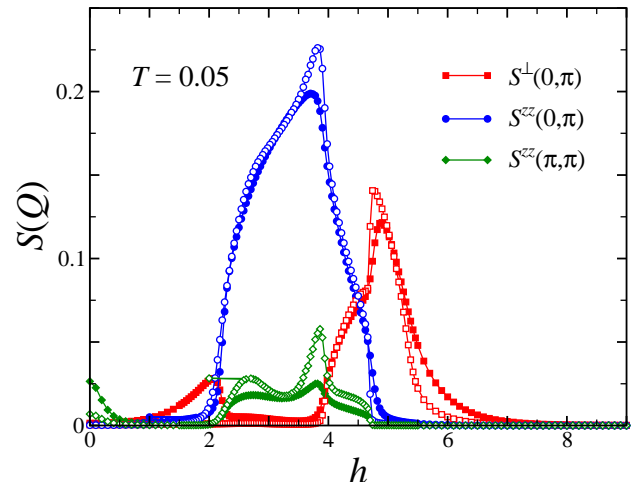


FIG. 4. The field variation of the longitudinal S^{zz} and transverse S^{\perp} spin-spin correlations at $\mathbf{Q}_{\text{Néel}} = (\pi, \pi)$ and $\mathbf{Q}_{\text{str}} = (0, \pi)$ [summed with $(\pi, 0)$] obtained for lattices with linear sizes $L = 32$ (closed symbols) and $L = 64$ (open symbols).

the *uuud* phase, respectively. The two noncollinear states possess the longitudinal LRO in the s^z components accompanied by the quasi-LRO in transverse spin components. Mapping this from magnetic to bosonic language [104], these two phases can be identified as supersolids, whereas the parent *uuud* phase is an insulating state with the density-wave crystal.

Figures 3 and 4 illustrate some of the data used in the construction of the phase diagram Fig. 2. First, let us consider the field derivative of the magnetization dm/dh . According to the analysis at the beginning of this section, at zero temperature $m(h)$ has a constant slope and

dm/dh remains flat for all fields below the saturation h_{sat} , *i.e.*, $dm/dh = J_1/8$ at $T = 0$ and for $h < h_{\text{sat}}$. At $T > 0$, we observe in Fig. 3 the emergence of small but sharp and distinct maxima, which may be taken as first indications of field-induced phase transitions. For $h \lesssim 4J_1 = h_{\text{sat}}/2$, we observe a drop in dm/dh . The slope of the magnetization curve $m(h)$ remains finite and thus one does not find a strict plateau in the classical magnetization curve. Nevertheless, the reduced slope of the magnetization curve can be considered as a distinctive feature of the *uuud* phase.

To further characterize different phases, we look now at the static spin structure factor $S^{\alpha\beta}(\mathbf{Q})$:

$$S^{\alpha\beta}(\mathbf{Q}) = \frac{1}{N^2} \sum_{i,j} \langle s_i^\alpha s_j^\beta \rangle e^{i\mathbf{Q} \cdot (\mathbf{R}_i - \mathbf{R}_j)}, \quad (5)$$

where $N = L^2$ is the total number of sites and L is the linear size of a simulated lattice. Figure 4 shows the Monte Carlo results for two linear lattice sizes $L = 32$ and 64 to illustrate the role of finite-size effects. For the considered temperature $T/J_1 = 0.05$, the longitudinal static structure factor S^{zz} indicates presence of the long-range order both for $\mathbf{Q}_{\text{N\'eel}} = (\pi, \pi)$ and $\mathbf{Q}_{\text{str}} = (0, \pi)$, whereas the transverse structure factor S^\perp vanishes for $2 \lesssim h/J_1 \lesssim 4$. This is exactly the behavior expected for the *uuud* phase. For $4 \lesssim h/J_1 \lesssim 5$, we observe the coexistence of finite amplitudes both in S^{zz} and in $S^\perp(\mathbf{Q}_{\text{str}})$, exactly as expected for the 3:1 supersolid phase. In a striking contrast with the behavior expected from the toy biquadratic exchange model [93, 94], the supersolid 3:1 state does not extend all the way up to the saturation at $h = h_{\text{sat}}$. For $h/J_1 \lesssim 2$ and $h/J_1 \gtrsim 5$, Fig. 4 exhibits a signal in the transverse structure factor $S^\perp(\mathbf{Q}_{\text{str}})$, but none in the longitudinal one S^{zz} . Since this corresponds to breaking of a continuous rotational symmetry around the z axis, the resulting order can be only a quasi-LRO at $T > 0$ with algebraic decay of spin-spin correlations. Transitions out of these phases are expected to be in the Berezinskii-Kosterlitz-Thouless (BKT) universality class [105–107], and indeed, the order parameter S^\perp vanishes smoothly in Fig. 4 in the low- and high-field limit, respectively. An accurate determination of the BKT boundaries is beyond the scope of the present study. Instead, we indicate their presence on the phase diagram by grey regions in Fig. 2.

Figures 5 and 6 illustrate stability of the *uuud* state upon moving away from the strongly frustrated point $J_2 \neq 0.5J_1$. Focusing first on field scans in Fig. 5 for $T = 0.06J_1$, one can clearly observe sharp anomalies in the field derivative of the magnetization dm/dh for $J_2/J_1 = 0.5 \pm 0.005$ indicating the upper and lower boundaries of the the *uuud* plateau state. In contrast, dm/dh remains completely flat for $J_2/J_1 = 0.51$ featuring canted N\'eel and stripe states in the entire range of magnetic fields. For $T = 0.06J_1$ and $h = 3.6J_1$, Fig. 6 shows the dependence of the transverse and longitudinal components of the static structure factor upon varying the ratio of J_2/J_1 . Here, one can see the same trend

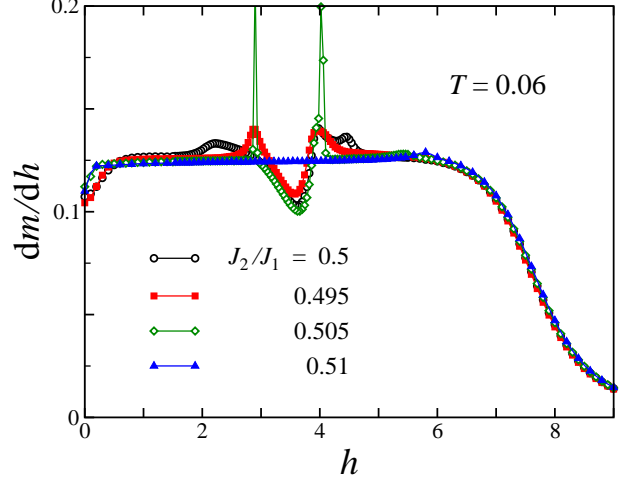


FIG. 5. Field derivative of magnetization for the classical FSAFM at $T = 0.06$ for different exchange ratios close to $J_2 = 0.5$ (in units of $J_1 = 1$).

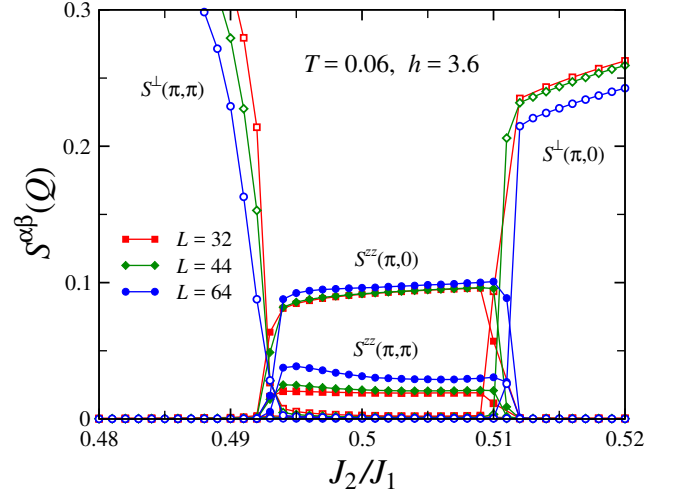


FIG. 6. Static structure factor of the classical FSAFM for fixed $T = 0.06$ and $h = 3.6$ (in units of $J_1 = 1$) as a function of J_2/J_1 for three lattice sizes L .

with the *uuud* state clearly stabilized by thermal fluctuations in a finite range of J_2/J_1 . Note that the *uuud* state is the classical ground state only for a single frustration ratio $J_2/J_1 = 1/2$. Hence, for $J_2/J_1 \neq 1/2$, the region of the *uuud* phase is detached from the vertical axis of the phase diagram at $T = 0$ and requires sufficiently strong thermal fluctuations for its stabilization. Conversely, for $J_2/J_1 = 1/2$ the strong thermal fluctuations for $T \gtrsim 0.1J_1$ destroy the *uuud* LRO, see Fig. 2. Thus, one requires a delicate balance of sufficiently but not too strong thermal fluctuations to stabilize the *uuud* state, consistent with its disappearance when J_2/J_1 deviates by about 0.01 from the degenerate ratio 1/2.

III. QUANTUM MODEL

We start with a basic consideration that is valid for any spin quantum number s : the single-magnon dispersion above the ferromagnetically polarized background is a single-particle problem that is straightforward to solve. One finds the single-magnon dispersion to be given by (compare also Ref. [73])

$$\begin{aligned} \omega(k_x, k_y) &= 2s(J_1(\cos k_x + \cos k_y) \\ &\quad + J_2(\cos(k_x + k_y) + \cos(k_x - k_y))) \\ &\quad - 4s(J_1 + J_2) + h \\ &= 2s(J_1(\cos k_x + \cos k_y) + 2J_2 \cos k_x \cos k_y) \\ &\quad - 4s(J_1 + J_2) + h. \end{aligned} \quad (6)$$

If the transition to saturation is a second-order quantum phase transition, the minimal single-magnon energy vanishes exactly at the saturation field $\omega(\mathbf{k}_{\min}) - h_{\text{sat}} = 0$. Applying this condition to Eq. (6), we can determine the saturation field as

$$h_{\text{sat}} = \begin{cases} 8sJ_1 & \text{for } J_2 \leq J_1/2, \\ 4s(J_1 + 2J_2) & \text{for } J_2 \geq J_1/2. \end{cases} \quad (7)$$

In particular $h_{\text{sat}} = 8sJ_1$ at $J_1 = J_2/2$. In the classical limit $s \rightarrow \infty$ and upon suitably rescaling the spins by $1/s$, *i.e.*, by effectively replacing $s \rightarrow 1$, we find $h_{\text{sat}} = 8J_1$ at $J_1 = J_2/2$ in the classical limit, as already stated in Subsec. II A.

An interesting special case is $J_2 = J_1/2$ where the dispersion relation (6) simplifies (see also Ref. [77])

$$\omega(k_x, k_y)|_{J_1=J_2/2} = 2sJ_1((1 + \cos k_x)(1 + \cos k_y) - 4) + h \quad (8)$$

such that

$$\omega(k_x, \pi)|_{J_1=J_2/2} = \omega(\pi, k_y)|_{J_1=J_2/2} = -8sJ_1 + h, \quad (9)$$

i.e., we find degenerate lines of minima for $h \geq h_{\text{sat}}$. This is reminiscent of the classical degeneracy discussed in Subsec. II A, in particular the degenerate manifold evolving from the *uuud* state at $m = 1/2$.

A. Zero-temperature $s = 1/2$ phase diagram

To numerically investigate the quantum case at finite magnetization $m < 1$, we now restrict to the extreme quantum limit $s = 1/2$. We employ the Lanczos method [108, 109] to find the minimal eigenvalues and -vectors of the Hamiltonian and thus determine its ground-state properties. We use in particular S^z conservation. The total Hilbert space for a given S^z and N spins $1/2$ has dimension $\binom{N}{N/2-S^z}$. Consequently, the dimension is maximal for $S^z = 0$ and decreases with increasing S^z , *i.e.*, higher magnetic fields. In particular, we can push computations to the $N = 52$ lattice shown in Fig. 7 for $m \gtrsim 1/2$,

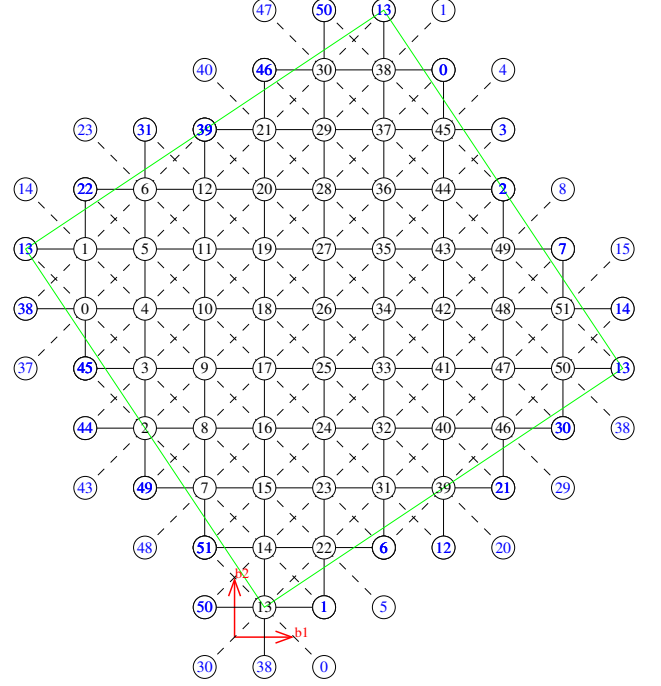


FIG. 7. The J_1 - J_2 model on a finite square lattice of $N = 52$ sites. Repeated sites (shown in blue) indicate periodic boundary conditions.

i.e., $S^z \gtrsim N/4 = 13$. This covers in particular the region relevant to a possible $m = 1/2$ plateau. Note that this $N = 52$ lattice shares the 90° rotational symmetry of the infinite lattice, but it breaks spatial reflection symmetries.

1. Magnetization curves

Figure 8 presents zero-temperature magnetization curves, where we normalized the saturation magnetization to $m = 1$. For reference, we include the plain square-lattice case with $J_2 = 0$ (Fig. 8(a)) that has been investigated in detail previously, see for example Ref. [111], including the $N = 40$ results. Here, we find a smooth curve in the thermodynamic limit with an upwards curvature that ends in a logarithmic singularity. This behavior is characteristic of a two-dimensional quantum spin system, and has been analytically predicted for the present case by second-order spin-wave theory [112].

Figure 8(b) presents the results for the highly frustrated case $J_2/J_1 = 1/2$. Here, we have no evidence for particular features around $m = 1/2$ and thus have drawn a smooth curve as estimate for the behavior in the limit $N \rightarrow \infty$. However, the transition to saturation is exceptionally steep in this case, as is demonstrated by the inset to Fig. 8(b). This behavior can be traced to the degeneracy of the one-magnon spectrum arising at $J_2/J_1 = 1/2$, see Eq. (9). This degeneracy gives rise to excitations lo-

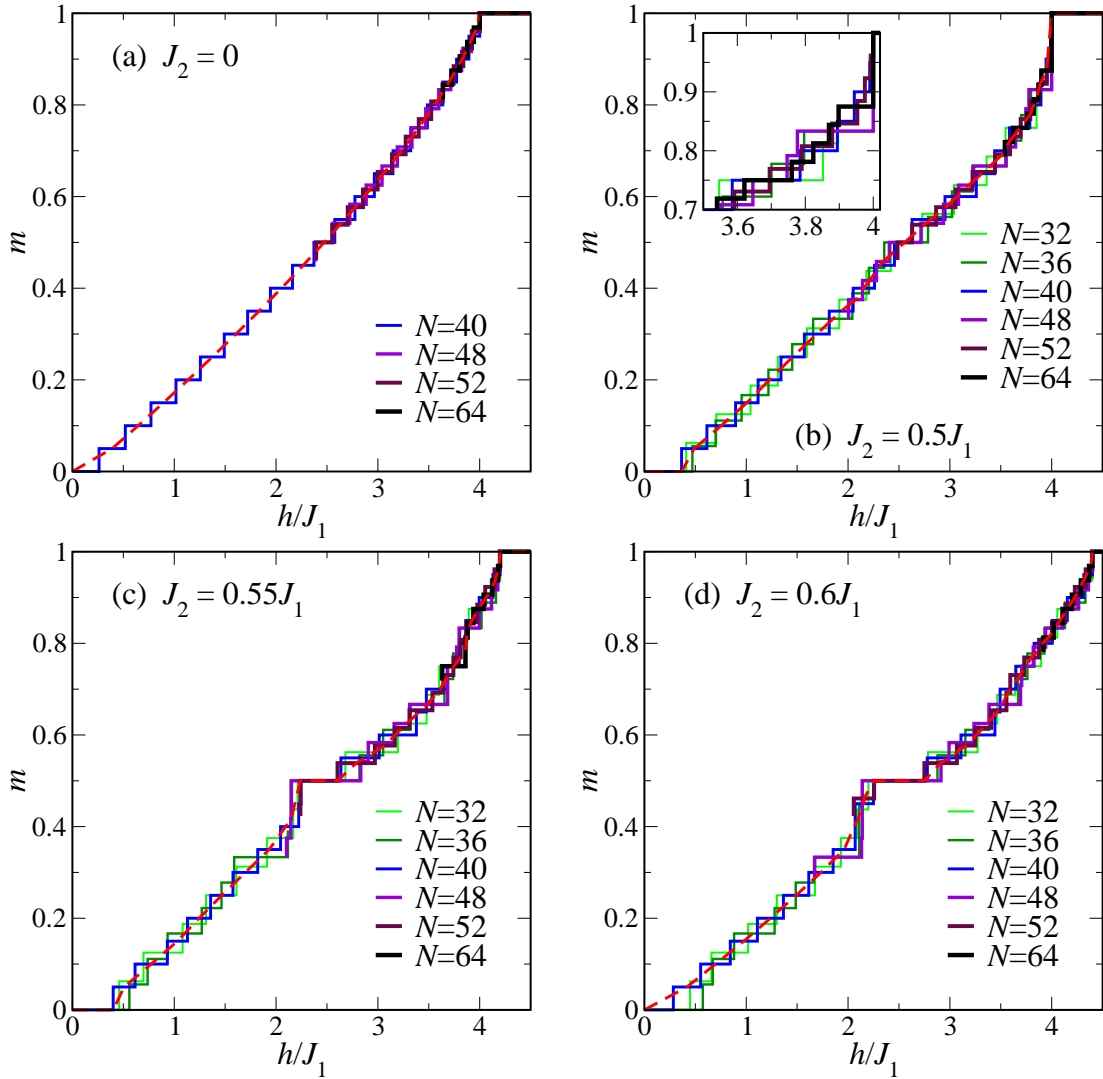


FIG. 8. Zero-temperature magnetization curves $m(h)$ of the spin-1/2 FSAFM for $J_2/J_1 = 0$ (a), 0.5 (b), 0.55 (c), and 0.6 (d). Full curves denote finite-size results for the given system size N . The dashed red lines indicate an estimate for the behavior of the infinite system. This estimate is obtained by connecting the midpoints of the finite-size steps for the largest available system size N [110], except for suspected plateaux (including the transition to saturation $m = 1$), where we use the corners of the steps instead. For a discussion why we draw $m = 1/2$ plateaux in the extrapolated curves at $J_2/J_1 = 0.55$ and 0.6, but none for $J_2/J_1 = 0.5$, compare Fig. 9 below and the discussion in the text; for the identification of this $m = 1/2$ plateau with the *uuud* state, see Fig. 10 below and the discussion in the text.

calized along horizontal or vertical lines across the lattice [75] and thus leads to a finite-size jump to saturation of size $\delta m = 1/L$ for an $L \times L$ square geometry. In the thermodynamic limit, this is expected to give rise to a square-root singularity with a logarithmic correction at the saturation field h_{sat} [77].

Next, we consider the case $J_2/J_1 = 0.55$, see Fig. 8(c). Here, the $N = 48$ system appears to be an outlier, but the other system sizes converge to a stable $m = 1/2$ plateau. The resulting magnetization curve is in good agreement with results from the density matrix renormalization group (DMRG) method [81], and even the estimates of the lower and upper critical fields of the

$m = 1/2$ plateau are in reasonable quantitative agreement. Note furthermore that the slope of the magnetization curve is very steep when it approaches $m = 1/2$ from below. This might be a signature of a first-order quantum phase transition, although the available data does not suffice to draw a definite conclusion on the nature of this field-induced phase transition.

Finally, we look at $J_2/J_1 = 0.6$. The resulting magnetization curve, shown in Fig. 8(d), is qualitatively similar to the case $J_2/J_1 = 0.55$. In particular, we find again an $m = 1/2$ plateau that might be even broader than in the previous case. Our results are again consistent with the DMRG ones [81] for $J_2/J_1 = 0.6$.

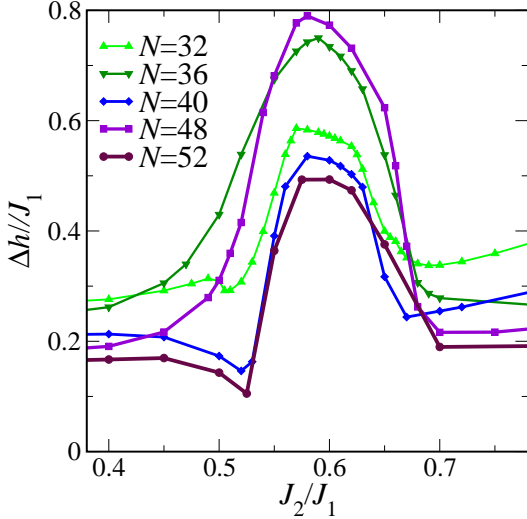


FIG. 9. Width Δh of the $m = 1/2$ step in the magnetization curve as a function of the frustration parameter J_2/J_1 . Symbols represent actual data points whereas lines are guides to the eye.

We note that a Chern-Simons theory predicted a distinct $m = 1/3$ plateau in addition to the $m = 1/2$ one [76]. The $N = 36$ and 48 systems indeed exhibit a broader step for $J_2/J_1 = 0.55$ (Fig. 8(c)) and 0.6 (Fig. 8(d)). However, the magnetization curves for the other system sizes appear to exhibit a smooth behavior in this region, the mean-field theory underlying the prediction of Ref. [76] is not well controlled, and the DMRG investigation Ref. [81] did not observe an $m = 1/3$ plateau either. We have therefore not drawn an $m = 1/3$ plateau in our extrapolated curves.

Lastly, we note that at $J_2/J_1 = 0.5$ and $J_2/J_1 = 0.55$ we have drawn an $m = 0$ plateau in Fig. 8(b) and (c), respectively. This corresponds to a spin gap in zero field, as is to be expected for the paramagnetic phases around $J_2/J_1 = 1/2$ mentioned in the Introduction. The situation for $J_2/J_1 = 0.6$ (Fig. 8(d)) is less clear. Here, the $N = 36$ system suggests the presence of a spin gap, but this is not confirmed by the $N = 40$ system. We therefore have not drawn an $m = 0$ plateau although we cannot exclude the existence of a small $m = 0$ plateau, *i.e.*, spin gap for $J_2/J_1 = 0.6$. In any case, we recall that the zero-field behavior is a challenging issue that is beyond the scope of the present work.

2. $m = 1/2$ plateau

Now we focus on a more detailed characterization of the $m = 1/2$ plateau. First, we look at the width of the $m = 1/2$ step, calculated as $\Delta h = E(N/2 + 1) - 2E(N/2) + E(N/2 - 1)$, where $E(S^z)$ is the energy of the ground state for the given value of S^z at $h = 0$. Figure 9 presents the behavior of Δh as a function of J_2/J_1 for

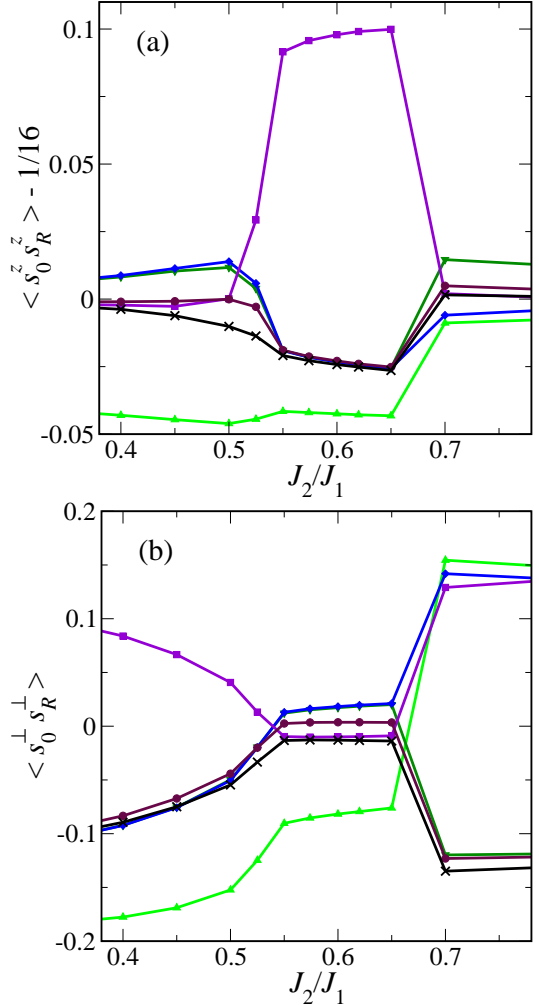


FIG. 10. Real-space correlations on the $N = 52$ lattice for $m = 1/2$ ($S^z = 13$) as a function of J_2/J_1 . Panel (a) shows the connected longitudinal correlations, panel (b) the transverse ones^a. Symbols represent actual data points whereas lines are guides to the eye.

^a Reliable information about the corresponding values of R is no longer available, as neither is the relevant author. We therefore refrain from labeling the curves and mention just that the same symbols and colors are used for transverse and longitudinal correlations at the same R .

systems with $32 \leq N \leq 52$ spins $1/2$. We have chosen lattices with an aspect ratios as close as possible to unity for a given size N , but nevertheless the results fall into two groups, namely the square respectively rectangular geometries for $N = 36$ and 48 on the one side, and the tilted cases $N = 32, 40$, and 52 on the other side. This non-monotonic finite-size behavior renders an extrapolation to $N \rightarrow \infty$ difficult. Nevertheless, we observe a clear and consistent enhancement of the $m = 1/2$ step size in the region $0.52 \lesssim J_2/J_1 \lesssim 0.7$, which we thus take as a first estimate for the stability region of the $m = 1/2$ plateau.

To gain further insight into the state of the $m = 1/2$ plateau, Fig. 10 shows real-space spin-spin correlations at distance R for the $N = 52$ lattice of Fig. 7, *i.e.*, at $S^z = 13$. Note that $\langle s_R^z \rangle = m/2 = 1/4$. We therefore subtract a background of $\langle s_0^z \rangle \langle s_R^z \rangle = 1/16$ from the longitudinal correlation function $\langle s_0^z s_R^z \rangle$ to obtain the connected one, that is shown in Fig. 10(a). The transverse one in Fig. 10(b) is obtained as $\langle s_0^\perp s_R^\perp \rangle = \langle \mathbf{s}_0 \cdot \mathbf{s}_R \rangle - \langle s_0^z s_R^z \rangle$. Overall, we observe three distinct regimes in Fig. 10: (i) For $J_2/J_1 \lesssim 0.5$ the transverse correlations dominate. This is consistent with Néel order in the transverse components, as expected in the limit $J_2 = 0$. (ii) For $0.52 \lesssim J_2/J_1 < 0.7$, the transverse correlations essentially vanish, but strong longitudinal ones develop. This is consistent with the collinear *uuud* state that is expected for an $m = 1/2$ plateau from the investigation of the classical model in Sec. II A. (iii) For $J_2/J_1 > 0.7$, the longitudinal components vanish again while a new signal develops in the transverse components. Different signs reflect an order that differs from the one in regime (i). Indeed, for $J_1 = 0$, one has two interpenetrating square lattices, each of which develops independent Néel order. A weak coupling $J_1 > 0$ then leads to a “stripe” phase, consistent with the correlations observed in Fig. 10(b) for $J_2/J_1 > 0.7$.

Taken together, the data for Δh and the spin-spin correlation functions at $m = 1/2$ are consistent with an *uuud* plateau in the regime $0.52 \lesssim J_2/J_1 \lesssim 0.7$, gapless transverse Néel order for $J_2/J_1 \lesssim 0.52$, and gapless transverse stripe order for $J_2/J_1 \gtrsim 0.7$. These results on the stability of the *uuud* state for the $s = 1/2$ model are in sharp contrast with the thermal order by disorder for classical spins obtained above in Sec. II. Specifically, for a fixed T the *uuud* state appears rather symmetrically for $0.492 \lesssim J_2/J_1 \lesssim 0.51$ in the classical model, see Fig. 6. In fact, this behavior illustrates a remarkable distinction between quantum and thermal order-by-disorder effects already mentioned in the end of Sec. II A. Using a so-called augmented spin-wave theory for large spins, Coletta *et al.* [80] have demonstrated such an asymmetric stabilization of the 1/2 plateau for $J_2/J_1 \gtrsim 0.5$. This effect is driven by the high-energy magnons with $\omega(\mathbf{k}) \approx J_s$, which contribute to the vacuum zero-point energy on the same footing with the low-energy magnons. On the other hand, the thermal order by disorder is completely dominated by the low-energy magnons with $\omega(\mathbf{k}) \approx T$.

B. Thermodynamics for $s = 1/2$

Finally, we investigate the finite-temperature behavior of the $s = 1/2$ FSAFM. This is motivated by two questions. Firstly, we are interested in the stability of the *uuud* state at finite temperature and secondly we intend to verify the impact of the competing interactions on the magnetocaloric effect, in particular around the degeneracy arising at the saturation field h_{sat} for $J_2/J_1 = 1/2$. To address these questions, we focus on the two cases

$J_2/J_1 = 0.5$ and 0.55 .

In order to obtain results for system sizes N that are comparable to those that we have investigated at $T = 0$, we employ the finite-temperature Lanczos method [113–123]. To be precise, we have employed two different implementations of this method. A first one follows the historic route [113, 114, 116–120] whereas a second one builds on the notion of “thermal pure quantum states” (TPQ) [124, 125]. With the Krylov approximation to the imaginary-time evolution [126], the two methods become equivalent [127], but the technical implementations are still different, and the second point of view lends a more solid theoretical foundation to the earlier heuristic approach. In order to distinguish the two methods, we refer to the historical approach as “FTLM” and to the more recent implementation [121] as “TPQ”.

1. Specific heat

Figure 11 presents the specific heat per spin C as a function of temperature at $J_2/J_1 = 0.55$ for two selected fields $h/J_1 = 4$ and 2.4 . TPQ and FTLM are subject to statistical errors that arise from sampling of the start vectors, corresponding to the $T = \infty$ limit. The cyan error tube around the $N = 36$ TPQ result has been obtained with a jackknife analysis [128], whereas no error bars are shown for the FTLM results in Fig. 11.

The first case $h/J_1 = 4$ lies just below the saturation field that is $h_{\text{sat}}/J_1 = 4.2$ for $J_2/J_1 = 0.55$ (see Eq. (7)). The result for the $N = 36$ system is shown in Fig. 11(a) and serves as a benchmark. The proximity to saturation permits us to perform exact diagonalization (ED) that covers the complete spectrum up to sufficiently high temperatures to yield essentially exact results for the entire temperature range shown. This ED curve is free from the statistical errors that are inherent to FTLM and thus serves as a reference. We see that the FTLM curve is very close to the ED one, and also the TPQ curve deviates from these two only by an amount that is consistent with the estimated error. The features observed in Fig. 11(a) around $T/J_1 = 0.01$ and 0.05 are most likely due to finite-size effects reflecting the finite system size $N = 36$ and thus have no physical meaning.

Figure 11(b) shows results for $h/J_1 = 2.4$. This value of the field is chosen to lie in the middle of the $m = 1/2$ plateau of the $T = 0$ magnetization curve, see Fig. 8(c). TPQ and FTLM for the $N = 36$ system are again consistent with each other. Beyond this, here we include results for other system sizes, namely $N = 24$ ED and also FTLM for $N = 40$ and 48 . We note that for $N \leq 40$ we have sampled all S^z sectors, but for $N = 48$ this is no longer possible. Validity of the $N = 48$ FTLM results is thus restricted to high magnetic fields and low temperatures. In particular for $h/J_1 = 2.4$, we have to restrict the $N = 48$ FTLM curve to $T/J_1 \leq 0.15$. Nevertheless, all curves in Fig. 11(b) exhibit a maximum in $C(T)$ around $T/J_1 \approx 0.1$. The system sizes studied here are

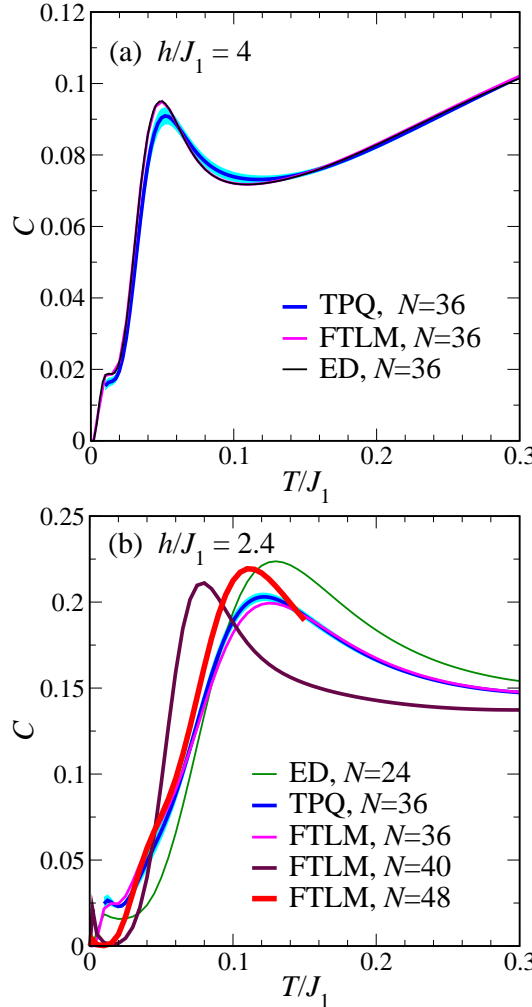


FIG. 11. Specific heat per spin of the $s = 1/2$ FSAFM at $J_2/J_1 = 0.55$ for $h/J_1 = 4$ (a) and $h/J_1 = 2.4$ (b). Panel (a) compares three different methods for the $N = 36$ system. Low-temperature features likely reflect the finite size of the system in this case. Panel (b) presents results for four different system sizes. In this case, features for $T \lesssim 0.02J_1$ are likely artifacts of either the finite size or the computational method whereas the peak for $T \approx 0.1J_1$ is taken as a signature of the phase transition into the $m = 1/2$ *uuud* state.

larger than those of previous investigations [83–88, 90], but they are still too small to permit an unambiguous determination of a thermodynamic phase transition. Nevertheless, the *uuud* state breaks translational symmetry such that we expect a finite-temperature phase transition out of it, as in the classical version of the model. The maxima of the specific heat in Fig. 11(b) may serve as an estimate for the location of the phase transition such that we infer a transition temperature of the order of $T = J_1/10$ for $h/J_1 = 2.4$. By contrast, the upturns observed at low temperature in the $N = 40$ and 48 FTLM curves are likely to be artifacts of the method, while the true low-temperature asymptotics of $C(T)$ is expected to

be an exponential decrease for $T \rightarrow 0$ on any system of a finite size N .

Finally, in Fig. 12 we show temperature-field scans of the specific heat per spin C (upper row of panels) and the entropy per spin S (lower row of panels) for $J_2/J_1 = 0.5$ (left column of panels) and $J_2/J_1 = 0.55$ (right column of panels). Here we have exploited the fact that the Hilbert space dimension decreases with increasing m to build a composite of different system sizes such that we start with $N = 40$ at low fields and increase N with increasing m and decreasing temperatures such that we reach $N = 400$ for $m \gtrsim 1$ at low temperatures.

According to Subec. III A 2, there should be no $m = 1/2$ plateau at $T = 0$ for $J_2/J_1 = 0.5$. If the case $s = 1/2$ is analogous to the classical case shown in Fig. 2, the maximum of C at $T/J_1 \approx 0.1$ for $1 \lesssim h/J_1 \gtrsim 2$ observed in Fig. 12(a) might nevertheless indicate a transition out of an *uuud* phase stabilized by thermal fluctuations. For $J_2/J_1 = 0.55$, we find an $m = 1/2$ plateau in the range of fields $2.24 \lesssim h/J_1 \lesssim 2.60$, see Fig. 8(c). The maximum of C for $T/J_1 \lesssim 0.1$ that one observes in this range of fields in Fig. 12(b) probably corresponds to a transition out of this plateau state, as we have discussed in the context of Fig. 11(b). Invoking again the analogy with the classical case Fig. 2, the continuation of this maximum to lower fields $1.2 \lesssim h/J_1 \lesssim 2.2$ and at $T/J_1 \lesssim 0.08$ might again correspond to a transition out of an *uuud* state stabilized by thermal fluctuations. This suggests an intriguing scenario where the crossover from stabilization by quantum to thermal fluctuations around $h/J_1 \approx 0.55$ would be accompanied by a minimum in the transition temperature.

In the low-field limit, the specific heat of Fig. 12(a,b) exhibits a maximum around $T/J_1 \approx 0.2$. It is an interesting question whether this is just a fluctuation maximum or a signature related to non-trivial ground states, but this question goes beyond the scope of the present work.

2. Entropy and magnetocaloric effect

We now turn to the entropy S that is shown in Fig. 12(c,d). This quantity and the related magnetocaloric effect were investigated previously in the classical case [88] and for spin 1/2 [85–87, 90]. However, these previous investigations of the spin-1/2 model were restricted to $N \leq 24$ and consequently to relatively high temperatures. Since the entropy is related to the specific heat C/T by an integral, the information content encoded in the entropy is equivalent to the specific heat that we discussed previously. In this respect, the $S = 0.05$ isentrope, *i.e.*, the leftmost white curve in Fig. 12(c,d) can be considered to roughly trace the expected transition into the *uuud* phase that we have discussed above. However, the entropy also yields a more direct access to the magnetocaloric effect, as the isentropes show the behavior of the system under adiabatic changes of the magnetic field. We observe distinct field-controlled cooling

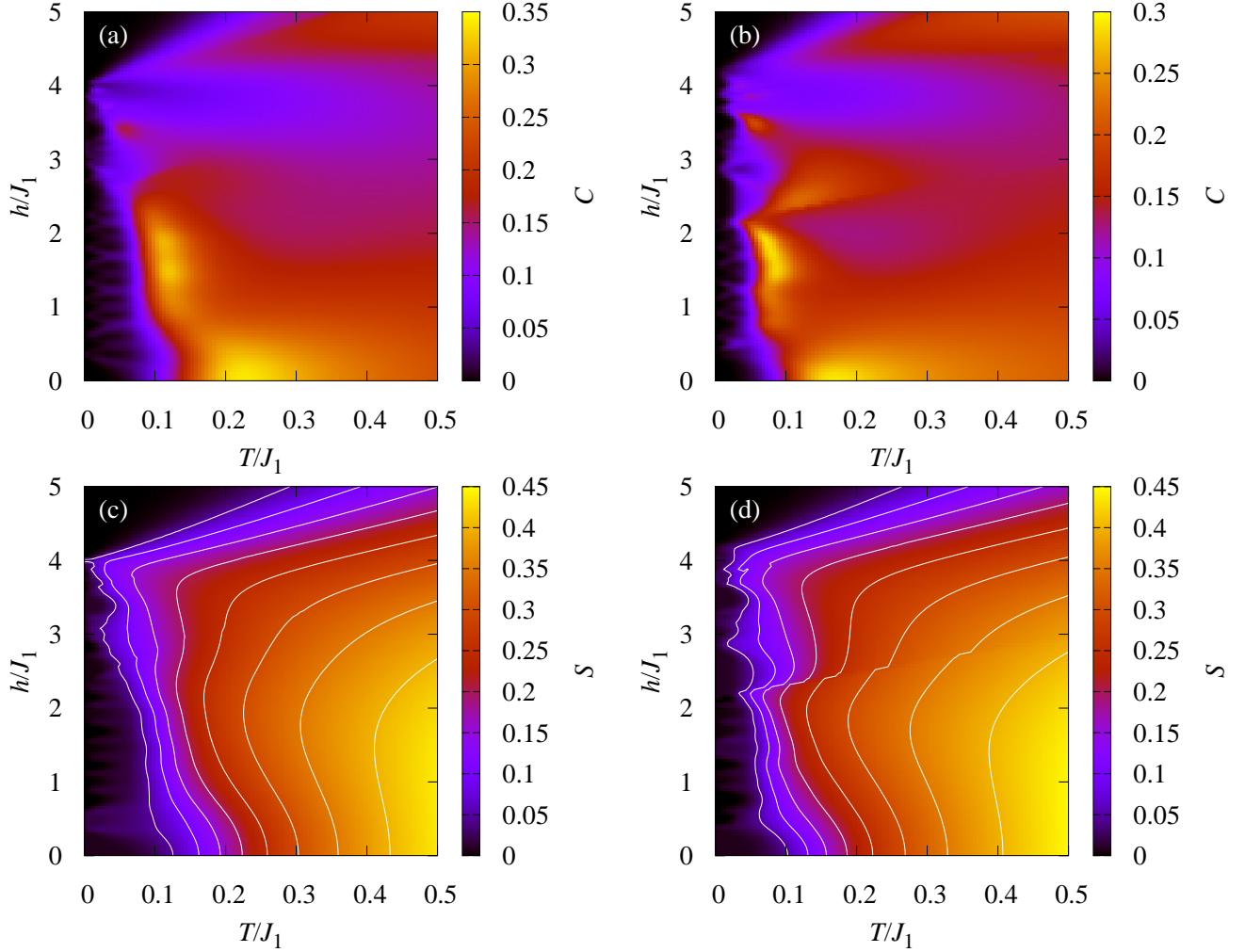


FIG. 12. Specific heat per spin C (a,b) and entropy per spin S (c,d) as a function of temperature and magnetic field for $J_2/J_1 = 0.5$ (a,c) and 0.55 (b,d). These figures are composites of different system sizes, starting with $N = 40$ for $m \lesssim 1/2$, going over $N = 48$ for $1/2 \lesssim m \lesssim 1$, $N = 64$ for $m \gtrsim 1$ at high T to $N = 400$ for $m \gtrsim 1$ at low T . The white solid lines in panels (c,d) trace values of constant entropy per spin. The leftmost curve is for $S = 0.05$, and S increases in steps of 0.05 with increasing temperature.

around the saturation field in Fig. 12(c,d) and close to the quantum-phase transitions [129, 130] terminating the $m = 1/2$ plateau in Fig. 12(d).

Geometric frustration is expected to enhance the magnetocaloric effect [130–133]. In the present case, we expect such an enhancement specifically at $J_2/J_1 = 1/2$ where the single-magnon spectrum becomes degenerate, recall Eq. (9). Such an enhancement was indeed observed in previous works [85, 86, 90] that scanned the ratio J_2/J_1 at a fixed temperature. Here, such an enhancement is observed as a pronounced minimum in the lowest three isentropes $T(h)$ around h_{sat} in Fig. 12(d).

IV. CONCLUSION

We have revisited the behavior of the J_1 - J_2 FSAFM in a magnetic field, pushing previous investigations [72–74] to bigger system sizes and higher accuracy.

We first determined the phase diagram of the classical Heisenberg model at $J_2/J_1 = 1/2$. Here, we confirmed order-by-disorder stabilization of the *uuud* state around half of the saturation field and for temperatures $0 < T \lesssim J_1/10$. In addition, we showed that 2:1:1 and 3:1 supersolid phases emerge below and above the *uuud* one, respectively. Furthermore, we provided evidence that the *uuud* phase persists in a small window around $J_2/J_1 = 1/2$, although the full phase diagram of the classical FSAFM remains to be investigated for $J_2/J_1 \neq 1/2$.

Then we turned to the spin-1/2 case. First, we pre-

sented zero-temperature magnetization curves for several ratios of J_2/J_1 and provided evidence for the emergence of an $m = 1/2$ plateau that can be understood as an *uuud* state stabilized by quantum fluctuations. We find a relatively large stabilization regime $0.52 \lesssim J_2/J_1 \lesssim 0.7$ that is shifted to values $J_2 > J_1/2$ such that analytic treatment of this *uuud* $m = 1/2$ plateau requires expansion around a classically unstable state [80]. Intriguingly, the *uuud* state is found to be stabilized by quantum fluctuations in the regime $h \gtrsim h_{\text{sat}}/2$, whereas the stabilization by thermal fluctuations takes place at lower fields $h \lesssim h_{\text{sat}}/2$. Such a trend is also known for the Heisenberg antiferromagnet on the triangular lattice, see, e.g., discussion in Ref. [102]. We expect that the supersolid phases found in the classical case below and above the *uuud* phase exist also for $s = 1/2$. While this expectation has been formulated earlier [74], a detailed investigation goes beyond the scope of the present work. Nevertheless, we mention that Ref. [81] found several non-trivial ordered states in the magnetization curves of the $s = 1/2$ FSAFM, although it is not entirely clear to us if their Y-like and V-like phases match our 2:1:1 and 3:1 states below and above the plateau, respectively.

Lastly, we computed finite-temperature properties of the $s = 1/2$ FSAFM in a magnetic field, relying mainly

on FTLM. We found preliminary signatures in the specific heat of a finite-temperature phase transition into the *uuud* state. Like in the classical case, these finite-temperature ordering transitions remain restricted to low temperatures $T/J_1 \lesssim 0.1$. We further observed that the degeneracy in the single-magnon spectrum at $J_2/J_1 = 1/2$ leads to an enhanced magnetocaloric effect at the saturation field.

ACKNOWLEDGMENTS

Johannes Richter was a prolific scientist. Regrettably, he did not witness completion of all of his projects. This is one of those that remained unfinished. Johannes Richter contributed the zero-temperature Lanczos calculations, part of the finite-temperature Lanczos results, and participated in the early stages of preparing the manuscript.

We are grateful to Jörg Schulenburg for providing `spinepack`, the code with which many of the computations were performed, and to Jürgen Schnack for sharing his insights on the finite-temperature Lanczos method.

The $N = 36$ TPQ computations were performed with a precursor of XDiag [134] using sublattice coding [135].

[1] C. Lhuillier and G. Misguich, Frustrated quantum magnets, in *High Magnetic Fields: Applications in Condensed Matter Physics and Spectroscopy*, edited by C. Berthier, L. P. Lévy, and G. Martinez (Springer Berlin Heidelberg, Berlin, Heidelberg, 2001) pp. 161–190.

[2] C. Lacroix, P. Mendels, and F. Mila, eds., *Introduction to Frustrated Magnetism*, Springer Series in Solid-State Sciences, Vol. 164 (Springer Berlin, Heidelberg, Berlin, Heidelberg, 2011).

[3] M. Inui, S. Doniach, and M. Gabay, Doping dependence of antiferromagnetic correlations in high-temperature superconductors, *Phys. Rev. B* **38**, 6631 (1988).

[4] P. Chandra and B. Doucot, Possible spin-liquid state at large S for the frustrated square Heisenberg lattice, *Phys. Rev. B* **38**, 9335 (1988).

[5] E. Dagotto and A. Moreo, Phase diagram of the frustrated spin-1/2 Heisenberg antiferromagnet in 2 dimensions, *Phys. Rev. Lett.* **63**, 2148 (1989).

[6] H. J. Schulz and T. A. L. Ziman, Finite-size scaling for the two-dimensional frustrated quantum Heisenberg antiferromagnet, *Europhys. Lett.* **18**, 355 (1992).

[7] H.J. Schulz, T.A.L. Ziman, and D. Poilblanc, Magnetic order and disorder in the frustrated quantum Heisenberg antiferromagnet in two dimensions, *J. Phys. I France* **6**, 675 (1996).

[8] J. Richter, Zero-temperature magnetic ordering in the inhomogeneously frustrated quantum Heisenberg antiferromagnet on a square lattice, *Phys. Rev. B* **47**, 5794 (1993).

[9] J. Richter, N. B. Ivanov, and K. Retzlaff, On the violation of Marshall-Peierls sign rule in the frustrated J_1 - J_2 Heisenberg antiferromagnet, *Europhys. Lett.* **25**, 545 (1994).

[10] M. E. Zhitomirsky and K. Ueda, Valence-bond crystal phase of a frustrated spin-1/2 square-lattice antiferromagnet, *Phys. Rev. B* **54**, 9007 (1996).

[11] A. E. Trumper, L. O. Manuel, C. J. Gazza, and H. A. Ceccatto, Schwinger-boson approach to quantum spin systems: Gaussian fluctuations in the “natural” gauge, *Phys. Rev. Lett.* **78**, 2216 (1997).

[12] R. F. Bishop, D. J. J. Farnell, and J. B. Parkinson, Phase transitions in the spin-half J_1 - J_2 model, *Phys. Rev. B* **58**, 6394 (1998).

[13] R. R. P. Singh, Z. Weihong, C. J. Hamer, and J. Oitmaa, Dimer order with striped correlations in the J_1 - J_2 Heisenberg model, *Phys. Rev. B* **60**, 7278 (1999).

[14] L. Capriotti, F. Becca, A. Parola, and S. Sorella, Resonating valence bond wave functions for strongly frustrated spin systems, *Phys. Rev. Lett.* **87**, 097201 (2001).

[15] O. P. Sushkov, J. Oitmaa, and Z. Weihong, Quantum phase transitions in the two-dimensional J_1 - J_2 model, *Phys. Rev. B* **63**, 104420 (2001).

[16] L. Siurakshina, D. Ihle, and R. Hayn, Magnetic order and finite-temperature properties of the two-dimensional frustrated Heisenberg model, *Phys. Rev. B* **64**, 104406 (2001).

[17] J. Sirker, Z. Weihong, O. P. Sushkov, and J. Oitmaa, J_1 - J_2 model: First-order phase transition versus deconfinement of spinons, *Phys. Rev. B* **73**, 184420 (2006).

[18] D. Schmalfuß, R. Darradi, J. Richter, J. Schulenburg, and D. Ihle, Quantum J_1 - J_2 antiferromagnet on a stacked square lattice: Influence of the interlayer coupling on the ground-state magnetic ordering, *Phys. Rev.*

Lett. **97**, 157201 (2006).

[19] M. Mambrini, A. Läuchli, D. Poilblanc, and F. Mila, Plaquette valence-bond crystal in the frustrated Heisenberg quantum antiferromagnet on the square lattice, *Phys. Rev. B* **74**, 144422 (2006).

[20] R. Darradi, O. Derzhko, R. Zinke, J. Schulenburg, S. E. Krüger, and J. Richter, Ground state phases of the spin-1/2 J_1 - J_2 Heisenberg antiferromagnet on the square lattice: A high-order coupled cluster treatment, *Phys. Rev. B* **78**, 214415 (2008).

[21] L. Isaev, G. Ortiz, and J. Dukelsky, Hierarchical mean-field approach to the J_1 - J_2 Heisenberg model on a square lattice, *Phys. Rev. B* **79**, 024409 (2009).

[22] V. Murg, F. Verstraete, and J. I. Cirac, Exploring frustrated spin systems using projected entangled pair states, *Phys. Rev. B* **79**, 195119 (2009).

[23] J. Richter and J. Schulenburg, The spin-1/2 J_1 - J_2 Heisenberg antiferromagnet on the square lattice: Exact diagonalization for $N=40$ spins, *Eur. Phys. J. B* **73**, 117 (2010).

[24] J. Reuther and P. Wölfle, J_1 - J_2 frustrated two-dimensional Heisenberg model: Random phase approximation and functional renormalization group, *Phys. Rev. B* **81**, 144410 (2010).

[25] B. Schmidt, M. Siahatgar, and P. Thalmeier, Ordered moment in the anisotropic and frustrated square lattice Heisenberg model, *Phys. Rev. B* **83**, 075123 (2011).

[26] J.-F. Yu and Y.-J. Kao, Spin- $\frac{1}{2}$ J_1 - J_2 Heisenberg antiferromagnet on a square lattice: A plaquette renormalized tensor network study, *Phys. Rev. B* **85**, 094407 (2012).

[27] H.-C. Jiang, H. Yao, and L. Balents, Spin liquid ground state of the spin- $\frac{1}{2}$ square J_1 - J_2 Heisenberg model, *Phys. Rev. B* **86**, 024424 (2012).

[28] T. Li, F. Becca, W. Hu, and S. Sorella, Gapped spin-liquid phase in the J_1 - J_2 Heisenberg model by a bosonic resonating valence-bond ansatz, *Phys. Rev. B* **86**, 075111 (2012).

[29] L. Wang, D. Poilblanc, Z.-C. Gu, X.-G. Wen, and F. Verstraete, Constructing a gapless spin-liquid state for the spin-1/2 J_1 - J_2 Heisenberg model on a square lattice, *Phys. Rev. Lett.* **111**, 037202 (2013).

[30] W.-J. Hu, F. Becca, A. Parola, and S. Sorella, Direct evidence for a gapless Z_2 spin liquid by frustrating Néel antiferromagnetism, *Phys. Rev. B* **88**, 060402 (2013).

[31] X. Zhang and K. S. D. Beach, Resonating valence bond trial wave functions with both static and dynamically determined Marshall sign structure, *Phys. Rev. B* **87**, 094420 (2013).

[32] S.-S. Gong, W. Zhu, D. N. Sheng, O. I. Motrunich, and M. P. A. Fisher, Plaquette ordered phase and quantum phase diagram in the spin- $\frac{1}{2}$ J_1 - J_2 square Heisenberg model, *Phys. Rev. Lett.* **113**, 027201 (2014).

[33] R. L. Doretto, Plaquette valence-bond solid in the square-lattice J_1 - J_2 antiferromagnet Heisenberg model: A bond operator approach, *Phys. Rev. B* **89**, 104415 (2014).

[34] Y.-Z. Ren, N.-H. Tong, and X.-C. Xie, Cluster mean-field theory study of J_1 - J_2 Heisenberg model on a square lattice, *J. Phys.: Condens. Matter* **26**, 115601 (2014).

[35] L. Wang, Correlated valence bond state and its study of the spin-1/2 J_1 - J_2 Anti-ferromagnetic Heisenberg model on a square lattice, ArXiv e-prints (2014), arXiv:1402.3564 [cond-mat.str-el].

[36] C.-P. Chou and H.-Y. Chen, Simulating a two-dimensional frustrated spin system with fermionic resonating-valence-bond states, *Phys. Rev. B* **90**, 041106 (2014).

[37] J. Richter, R. Zinke, and D. J. J. Farnell, The spin-1/2 square-lattice J_1 - J_2 model: the spin-gap issue, *Eur. Phys. J. B* **88**, 2 (2015).

[38] L. Wang, Z.-C. Gu, F. Verstraete, and X.-G. Wen, Tensor-product state approach to spin- $\frac{1}{2}$ square J_1 - J_2 antiferromagnetic Heisenberg model: Evidence for deconfined quantum criticality, *Phys. Rev. B* **94**, 075143 (2016).

[39] M. Rück and J. Reuther, Effects of two-loop contributions in the pseudofermion functional renormalization group method for quantum spin systems, *Phys. Rev. B* **97**, 144404 (2018).

[40] L. Wang and A. W. Sandvik, Critical level crossings and gapless spin liquid in the square-lattice spin-1/2 J_1 - J_2 Heisenberg antiferromagnet, *Phys. Rev. Lett.* **121**, 107202 (2018).

[41] R. Haghshenas and D. N. Sheng, $U(1)$ -symmetric infinite projected entangled-pair states study of the spin-1/2 square J_1 - J_2 Heisenberg model, *Phys. Rev. B* **97**, 174408 (2018).

[42] D. Poilblanc and M. Mambrini, Quantum critical phase with infinite projected entangled paired states, *Phys. Rev. B* **96**, 014414 (2017).

[43] R. Haghshenas, W.-W. Lan, S.-S. Gong, and D. N. Sheng, Quantum phase diagram of spin-1 J_1 - J_2 Heisenberg model on the square lattice: An infinite projected entangled-pair state and density matrix renormalization group study, *Phys. Rev. B* **97**, 184436 (2018).

[44] W.-Y. Liu, S. Dong, C. Wang, Y. Han, H. An, G.-C. Guo, and L. He, Gapless spin liquid ground state of the spin- $\frac{1}{2}$ J_1 - J_2 Heisenberg model on square lattices, *Phys. Rev. B* **98**, 241109 (2018).

[45] B. Zhao, J. Takahashi, and A. W. Sandvik, Comment on “Gapless spin liquid ground state of the spin- $\frac{1}{2}$ J_1 - J_2 Heisenberg model on square lattices”, *Phys. Rev. B* **101**, 157101 (2020).

[46] W.-Y. Liu, S. Dong, C. Wang, Y. Han, H. An, G.-C. Guo, and L. He, Reply to “Comment on ‘Gapless spin liquid ground state of the spin- $\frac{1}{2}$ J_1 - J_2 Heisenberg model on square lattices’”, *Phys. Rev. B* **101**, 157102 (2020).

[47] J. Hasik, D. Poilblanc, and F. Becca, Investigation of the Néel phase of the frustrated Heisenberg antiferromagnet by differentiable symmetric tensor networks, *SciPost Phys.* **10**, 012 (2021).

[48] Y. Nomura and M. Imada, Dirac-type nodal spin liquid revealed by refined quantum many-body solver using neural-network wave function, correlation ratio, and level spectroscopy, *Phys. Rev. X* **11**, 031034 (2021).

[49] W.-Y. Liu, J. Hasik, S.-S. Gong, D. Poilblanc, W.-Q. Chen, and Z.-C. Gu, Emergence of gapless quantum spin liquid from deconfined quantum critical point, *Phys. Rev. X* **12**, 031039 (2022).

[50] W.-Y. Liu, S.-S. Gong, Y.-B. Li, D. Poilblanc, W.-Q. Chen, and Z.-C. Gu, Gapless quantum spin liquid and global phase diagram of the spin-1/2 J_1 - J_2 square antiferromagnetic Heisenberg model, *Sci. Bull.* **67**, 1034 (2022).

[51] C. Roth, A. Szabó, and A. H. MacDonald, High-accuracy variational Monte Carlo for frustrated magnets with deep neural networks, *Phys. Rev. B* **108**, 054410

(2023).

[52] X. Qian and M. Qin, Absence of spin liquid phase in the J_1 - J_2 Heisenberg model on the square lattice, *Phys. Rev. B* **109**, L161103 (2024).

[53] A. Rückriegel, D. Tarasevych, and P. Kopietz, Phase diagram of the J_1 - J_2 quantum Heisenberg model for arbitrary spin, *Phys. Rev. B* **109**, 184410 (2024).

[54] H.-Y. Lin, Y. Guo, R.-Q. He, Z. Y. Xie, and Z.-Y. Lu, Green's function Monte Carlo combined with projected entangled pair state approach to the frustrated J_1 - J_2 Heisenberg model, *Phys. Rev. B* **109**, 235133 (2024).

[55] J. Huang, X. Qian, and M. Qin, Plaquette-type valence bond solid state in the J_1 - J_2 square-lattice Heisenberg model, *Phys. Rev. B* **110**, 195111 (2024).

[56] P. M. Vecsei and J. L. Lado, Phase diagram of the J_1 - J_2 heisenberg second-order topological quantum magnet, *Phys. Rev. Res.* **7**, 013194 (2025).

[57] X. Qian, R. Lv, J. Y. Lee, and M. Qin, From the Shastry-Sutherland model to the J_1 - J_2 Heisenberg model, *Phys. Rev. B* **111**, L241113 (2025).

[58] H.-K. Jin, H.-H. Tu, and Y.-H. Zhang, Dirac and chiral spin liquids on spin-1/2 square-lattice Heisenberg antiferromagnet, *Phys. Rev. B* **112**, 035159 (2025).

[59] J. Qiao, S.-H. Zhang, J.-B. Qin, X.-L. Zhao, and Q. Cheng, Phase transitions in the spin-1/2 Heisenberg antiferromagnet on the square lattice (2025), [arXiv:2511.06423 \[cond-mat.str-el\]](https://arxiv.org/abs/2511.06423).

[60] P. Carretta, N. Papinutto, C. B. Azzoni, M. C. Mozzati, E. Pavarini, S. Gonthier, and P. Millet, Frustration-driven structural distortion in VOMoO₄, *Phys. Rev. B* **66**, 094420 (2002).

[61] R. Melzi, P. Carretta, A. Lascialfari, M. Mambrini, M. Troyer, P. Millet, and F. Mila, Li₂VO(Si,Ge)O₄, a prototype of a two-dimensional frustrated quantum Heisenberg antiferromagnet, *Phys. Rev. Lett.* **85**, 1318 (2000).

[62] R. Melzi, S. Aldrovandi, F. Tedoldi, P. Carretta, P. Millet, and F. Mila, Magnetic and thermodynamic properties of Li₂VOSiO₄: A two-dimensional $S = 1/2$ frustrated antiferromagnet on a square lattice, *Phys. Rev. B* **64**, 024409 (2001).

[63] H. Rosner, R. R. P. Singh, W. H. Zheng, J. Oitmaa, and W. E. Pickett, High-temperature expansions for the J_1 - J_2 Heisenberg models: Applications to *ab initio* calculated models for Li₂VOSiO₄ and Li₂VOGeO₄, *Phys. Rev. B* **67**, 014416 (2003).

[64] K. Y. Povarov, V. K. Bhartiya, Z. Yan, and A. Zheludev, Thermodynamics of a frustrated quantum magnet on a square lattice, *Phys. Rev. B* **99**, 024413 (2019).

[65] H. Takeda, T. Yamauchi, M. Takigawa, H. Ishikawa, and Z. Hiroi, Pressure-induced phase transition in the J_1 - J_2 square lattice antiferromagnet RbMoOPO₄Cl, *Phys. Rev. B* **103**, 104406 (2021).

[66] M. Watanabe, N. Kurita, H. Tanaka, W. Ueno, K. Matsui, T. Goto, and M. Fujihala, Contrasting magnetic structures in SrLaCuSbO₆ and SrLaCuNbO₆: Spin- $\frac{1}{2}$ quasi-square-lattice J_1 - J_2 Heisenberg antiferromagnets, *Phys. Rev. B* **105**, 054414 (2022).

[67] S. Guchhait, D. V. Ambika, Q.-P. Ding, M. Uhlharz, Y. Furukawa, A. A. Tsirlin, and R. Nath, Deformed spin- $\frac{1}{2}$ square lattice in antiferromagnetic NaZnVOPO₄(HPO₄), *Phys. Rev. B* **106**, 024426 (2022).

[68] P. Park, G. Sala, T. Proffen, M. B. Stone, A. D. Christianson, and A. F. May, Quantum magnetism in the frustrated square lattice oxyhalides YbBi₂IO₄ and YbBi₂ClO₄, *Phys. Rev. B* **109**, 014426 (2024).

[69] M. Fujihala, M. Hagihala, A. Koda, J. G. Nakamura, A. Matsuo, K. Kindo, and M. Ishikado, Possible field-induced quantum state in a rhombic lattice antiferromagnet KCoPO₄·H₂O, *Phys. Rev. Mater.* **9**, 014406 (2025).

[70] X.-L. Xu, Y. Wang, L. Xu, Y. Li, and X. Li, Low-dimensional quantum antiferromagnetism in frustrated potassium 3d transition metal (II) phosphates: Insights from experimental and first-principles investigations, *J. Appl. Phys.* **137**, 173904 (2025).

[71] M. S. Yang and K. H. Mütter, The two dimensional antiferromagnetic Heisenberg model in the presence of an external field, *Z. Phys. B* **104**, 117 (1997).

[72] M. E. Zhitomirsky, A. Honecker, and O. A. Petrenko, Field induced ordering in highly frustrated antiferromagnets, *Phys. Rev. Lett.* **85**, 3269 (2000).

[73] A. Honecker, Lanczos study of the $S = 1/2$ frustrated square-lattice anti-ferromagnet in a magnetic field, *Can. J. Phys.* **79**, 1557 (2001).

[74] A. Honecker, O. Petrenko, and M. Zhitomirsky, Field-induced order and magnetization plateaux in frustrated antiferromagnets, *Physica B* **312-313**, 609 (2002).

[75] J. Schulenburg, A. Honecker, J. Schnack, J. Richter, and H.-J. Schmidt, Macroscopic magnetization jumps due to independent magnons in frustrated quantum spin lattices, *Phys. Rev. Lett.* **88**, 167207 (2002).

[76] M.-C. Chang and M.-F. Yang, Chern-Simons theory for magnetization plateaus of the frustrated J_1 - J_2 Heisenberg model, *Phys. Rev. B* **66**, 184416 (2002).

[77] G. Jackeli and M. E. Zhitomirsky, Frustrated antiferromagnets at high fields: Bose-Einstein condensation in degenerate spectra, *Phys. Rev. Lett.* **93**, 017201 (2004).

[78] N. Shannon, T. Momoi, and P. Sindzingre, Nematic order in square lattice frustrated ferromagnets, *Phys. Rev. Lett.* **96**, 027213 (2006).

[79] P. Thalmeier, M. E. Zhitomirsky, B. Schmidt, and N. Shannon, Quantum effects in magnetization of J_1 - J_2 square lattice antiferromagnet, *Phys. Rev. B* **77**, 104441 (2008).

[80] T. Coletta, M. E. Zhitomirsky, and F. Mila, Quantum stabilization of classically unstable plateau structures, *Phys. Rev. B* **87**, 060407(R) (2013).

[81] K. Morita and N. Shibata, Field-induced quantum phase transitions in $S = 1/2$ J_1 - J_2 Heisenberg model on square lattice, *J. Phys. Soc. Jpn.* **85**, 094708 (2016).

[82] H. Yamaguchi, Y. Sasaki, T. Okubo, M. Yoshida, T. Kida, M. Hagiwara, Y. Kono, S. Kittaka, T. Sakakibara, M. Takigawa, Y. Iwasaki, and Y. Hosokoshi, Field-enhanced quantum fluctuation in an $S = \frac{1}{2}$ frustrated square lattice, *Phys. Rev. B* **98**, 094402 (2018).

[83] N. Shannon, B. Schmidt, K. Penc, and P. Thalmeier, Finite temperature properties and frustrated ferromagnetism in a square lattice Heisenberg model, *Eur. Phys. J. B* **38**, 599 (2004).

[84] B. Schmidt and P. Thalmeier, Third-order magnetic susceptibility of the frustrated square-lattice antiferromagnet, *Physica B* **359-361**, 1387 (2005).

[85] B. Schmidt, N. Shannon, and P. Thalmeier, Two-dimensional frustrated spin systems in high magnetic fields, *J. Phys.: Conf. Ser.* **51**, 207 (2006).

[86] B. Schmidt, P. Thalmeier, and N. Shannon, Magnetocaloric effect in the frustrated square lattice J_1 - J_2

model, *Phys. Rev. B* **76**, 125113 (2007).

[87] B. Schmidt, N. Shannon, and P. Thalmeier, The frustrated $J_1 - J_2$ model in high magnetic fields, *J. Phys.: Condens. Matter* **19**, 145211 (2007).

[88] L. Seabra, N. Shannon, P. Sindzingre, T. Momoi, B. Schmidt, and P. Thalmeier, Two dimensional frustrated magnets in high magnetic field, *J. Phys.: Conf. Ser.* **145**, 012075 (2009).

[89] A. Mikheyenkov, A. Shvartsberg, V. Valiulin, and A. Barabanov, Thermodynamic properties of the 2D frustrated Heisenberg model for the entire J_1-J_2 circle, *J. Magn. Magn. Mater.* **419**, 131 (2016).

[90] B. Schmidt and P. Thalmeier, Frustrated two dimensional quantum magnets, *Phys. Rep.* **703**, 1 (2017).

[91] P. Prelovšek, K. Morita, T. Tohyama, and J. Herbrych, Vanishing Wilson ratio as the hallmark of quantum spin-liquid models, *Phys. Rev. Res.* **2**, 023024 (2020).

[92] M. E. Zhitomirsky, Real-space perturbation theory for frustrated magnets: application to magnetization plateaus, *J. Phys.: Conf. Ser.* **592**, 012110 (2014).

[93] M. T. Heinilä and A. S. Oja, Selection of the ground state in type-I fcc antiferromagnets in an external magnetic field, *Phys. Rev. B* **48**, 7227 (1993).

[94] K. Penc, N. Shannon, and H. Shiba, Half-magnetization plateau stabilized by structural distortion in the antiferromagnetic Heisenberg model on a pyrochlore lattice, *Phys. Rev. Lett.* **93**, 197203 (2004).

[95] J. Villain, R. Bidaux, J.-P. Carton, and R. Conte, Order as an effect of disorder, *J. Phys. France* **41**, 1263 (1980).

[96] E. F. Shender, Antiferromagnetic garnets with fluctuationally interacting sublattices, *Sov. Phys. JETP* **56**, 178 (1982).

[97] E. Rastelli, L. Reatto, and A. Tassi, Degenerate helimagnetic states, lines of soft modes and absence of long-range order in three dimensions, *J. Phys. C* **16**, L331 (1983).

[98] H. Kawamura, Spin-wave analysis of the antiferromagnetic plane rotator model on the triangular lattice—symmetry breaking in a magnetic field, *J. Phys. Soc. Jpn.* **53**, 2452 (1984).

[99] C. L. Henley, Ordering due to disorder in a frustrated vector antiferromagnet, *Phys. Rev. Lett.* **62**, 2056 (1989).

[100] E. F. Shender and P. C. W. Holdsworth, Order by disorder and topology in frustrated magnetic systems, in *Fluctuations and Order: The New Synthesis*, edited by M. Millonas (Springer US, New York, NY, 1996) pp. 259–279.

[101] M. E. Zhitomirsky, Octupolar ordering of classical kagome antiferromagnets in two and three dimensions, *Phys. Rev. B* **78**, 094423 (2008).

[102] M. V. Gvozdikova, P.-E. Melchy, and M. E. Zhitomirsky, Magnetic phase diagrams of classical triangular and kagome antiferromagnets, *J. Phys.: Condens. Matter* **23**, 164209 (2011).

[103] A. S. Gubina, T. Ziman, and M. E. Zhitomirsky, Fully frustrated octahedral antiferromagnets: Emergent complexity in external field, *Phys. Rev. B* **111**, L180411 (2025).

[104] T. Matsubara and H. Matsuda, A lattice model of liquid helium, I, *Prog. Theor. Phys.* **16**, 569 (1956).

[105] V. L. Berezinskii, Destruction of long-range order in one-dimensional and two-dimensional systems having a continuous symmetry group I. Classical systems, *Sov. Phys. JETP* **32**, 493 (1971).

[106] J. M. Kosterlitz and D. J. Thouless, Ordering, metastability and phase transitions in two-dimensional systems, *J. Phys. C* **6**, 1181 (1973).

[107] J. M. Kosterlitz, The critical properties of the two-dimensional xy model, *J. Phys. C* **7**, 1046 (1974).

[108] C. Lanczos, An iteration method for the solution of the eigenvalue problem of linear differential and integral operators, *J. Res. Natl. Bur. Stand.* **45**, 255 (1950).

[109] J. K. Cullum and R. A. Willoughby, *Lanczos Algorithms for Large Symmetric Eigenvalue Computations* (SIAM, 2002).

[110] J. C. Bonner and M. E. Fisher, Linear magnetic chains with anisotropic coupling, *Phys. Rev.* **135**, A640 (1964).

[111] A. Honecker, J. Schulenburg, and J. Richter, Magnetization plateaus in frustrated antiferromagnetic quantum spin models, *J. Phys.: Condens. Matter* **16**, S749 (2004).

[112] M. E. Zhitomirsky and T. Nikuni, Magnetization curve of a square-lattice Heisenberg antiferromagnet, *Phys. Rev. B* **57**, 5013 (1998).

[113] J. Jaklič and P. Prelovšek, Finite-temperature conductivity in the planar t - J model, *Phys. Rev. B* **50**, 7129 (1994).

[114] J. Jaklič and P. Prelovšek, Finite-temperature properties of doped antiferromagnets, *Adv. Phys.* **49**, 1 (2000).

[115] A. Hams and H. De Raedt, Fast algorithm for finding the eigenvalue distribution of very large matrices, *Phys. Rev. E* **62**, 4365 (2000).

[116] J. Schnack and O. Wendland, Properties of highly frustrated magnetic molecules studied by the finite-temperature Lanczos method, *Eur. Phys. J. B* **78**, 535 (2010).

[117] P. Prelovšek and J. Bonča, Ground state and finite temperature lanczos methods, in *Strongly Correlated Systems: Numerical Methods*, edited by A. Avella and F. Mancini (Springer Berlin Heidelberg, 2013) pp. 1–30.

[118] O. Hanebaum and J. Schnack, Advanced finite-temperature Lanczos method for anisotropic spin systems, *Eur. Phys. J. B* **87**, 194 (2014).

[119] P. Prelovšek, The finite temperature Lanczos method and its applications, in *The Physics of Correlated Insulators, Metals, and Superconductors*, Modeling and Simulation, Vol. 7, edited by E. Pavarini, E. Koch, R. Scalettar, and R. Martin (Verlag des Forschungszentrum Jülich, 2017) Chap. 7.

[120] J. Schnack, J. Schulenburg, and J. Richter, Magnetism of the $N = 42$ kagome lattice antiferromagnet, *Phys. Rev. B* **98**, 094423 (2018).

[121] A. Wietek, P. Corboz, S. Wessel, B. Normand, F. Mila, and A. Honecker, Thermodynamic properties of the Shastry-Sutherland model throughout the dimer-product phase, *Phys. Rev. Research* **1**, 033038 (2019).

[122] J. Schnack, J. Richter, and R. Steinigeweg, Accuracy of the finite-temperature Lanczos method compared to simple typicality-based estimates, *Phys. Rev. Research* **2**, 013186 (2020).

[123] K. Seki and S. Yunoki, Thermodynamic properties of an $S = \frac{1}{2}$ ring-exchange model on the triangular lattice, *Phys. Rev. B* **101**, 235115 (2020).

[124] S. Sugiura and A. Shimizu, Thermal pure quantum states at finite temperature, *Phys. Rev. Lett.* **108**, 240401 (2012).

[125] S. Sugiura and A. Shimizu, Canonical thermal pure

quantum state, *Phys. Rev. Lett.* **111**, 010401 (2013).

[126] M. Hochbruck and C. Lubich, On Krylov subspace approximations to the matrix exponential operator, *SIAM J. Numer. Anal.* **34**, 1911 (1997).

[127] A. Honecker, J. Richter, J. Schnack, and A. Wietek, Loop-gas description of the localized-magnon states on the kagome lattice with open boundary conditions, *Condensed Matter Physics* **23**, 43712 (2020).

[128] B. Efron and C. Stein, The jackknife estimate of variance, *Ann. Stat.* **9**, 586 (1981).

[129] L. Zhu, M. Garst, A. Rosch, and Q. Si, Universally diverging Grüneisen parameter and the magnetocaloric effect close to quantum critical points, *Phys. Rev. Lett.* **91**, 066404 (2003).

[130] B. Wolf, A. Honecker, W. Hofstetter, U. Tutsch, and M. Lang, Cooling through quantum criticality and many-body effects in condensed matter and cold gases, *Int. J. Mod. Phys. B* **28**, 1430017 (2014).

[131] M. E. Zhitomirsky, Enhanced magnetocaloric effect in frustrated magnets, *Phys. Rev. B* **67**, 104421 (2003).

[132] M. E. Zhitomirsky and A. Honecker, Magnetocaloric effect in one-dimensional antiferromagnets, *J. Stat. Mech.: Theor. Exp.* **2004**, P07012 (2004).

[133] A. Honecker and S. Wessel, Magnetocaloric effect in two-dimensional spin-1/2 antiferromagnets, *Physica B* **378-380**, 1098 (2006).

[134] A. Wietek, L. Staszewski, M. Ulaga, P. L. Ebert, H. Karlsson, S. Sarkar, H. Shackleton, A. Sinha, and R. D. Soares, XDiag: Exact diagonalization for quantum many-body systems (2025), [arXiv:2505.02901 \[cond-mat.str-el\]](https://arxiv.org/abs/2505.02901).

[135] A. Wietek and A. M. Läuchli, Sublattice coding algorithm and distributed memory parallelization for large-scale exact diagonalizations of quantum many-body systems, *Phys. Rev. E* **98**, 033309 (2018).